Journal of Magnetism and Magnetic Materials 322 (2010) 469–476

Contents lists available at ScienceDirect

Journal of Magnetism and Magnetic Materials

journal homepage: www.elsevier.com/locate/jmmm

On the accuracy of FFT based magnetostatic field evaluation schemes in micromagnetic hysteresis modeling

B. Van de Wiele [a,*], F. Olyslager [b], L. Dupré [a], D. De Zutter [b]

[a] Department of Electrical Energy, Systems and Automation, Ghent University, Sint Pietersnieuwstraat 41, B-9000 Ghent, Belgium
[b] Department of Information Technology, Ghent University, Sint Pietersnieuwstraat 41, B-9000 Ghent, Belgium

ARTICLE INFO

Article history:
Received 5 May 2009
Received in revised form
25 August 2009
Available online 7 October 2009

PACS:
75.40.Mg
75.60.−d

Keywords:
Hysteresis
Micromagnetism
Magnetostatic field

ABSTRACT

Micromagnetic hysteresis models for large, bulk like samples are useful for the identification of relations between microscopic material properties and macroscopic magnetic behavior. To bridge the gap between the nanometer space scale of the micromagnetic theory and the large sample dimensions, time and memory efficient numerical schemes are needed. In micromagnetic computations, fast Fourier transforms (FFTs) have been widely adopted to speed up magnetostatic field computations. In this paper, two FFT schemes are compared. The first scheme evaluates the magnetostatic field directly starting from the magnetization and has a large accuracy, while in the second scheme the magnetostatic field is derived from the scalar magnetic potential resulting in a reduced accuracy but also in a CPU time reduction for a magnetostatic field evaluation to 65% and a reduction of memory requirements to 55%. The influence of the low accuracy evaluations on the simulated macroscopic hysteresis behavior is studied. Therefore, comparison is made with the influence of thermal effects in hysteresis simulations. It is found that the resulting changes in macroscopic hysteresis behavior are of the same order of magnitude as the ones obtained when thermal fluctuations are taken into account in the high accuracy computations.

1. Introduction

The micromagnetic theory has been used to understand the fundamental magnetization processes on a microscopic space and time scale. Numerical micromagnetic schemes are, e.g. used successfully in the development of storage media. Now the growing computer resources open up the opportunity to apply the micromagnetic theory also to large, bulk like samples as electrical steels. Indeed, the magnetic dynamics in electrical steels used in machine cores and transformers is based on the same interactions as described by the micromagnetic theory. Since the exact material parameters (location of dislocations, interstitials, grain boundaries) are not known on a nanometer scale, the *exact* space and time localization of the internal magnetization processes is also much less important. One is predominantly interested in the resulting—averaged—macroscopic magnetic behavior and the determination of the dominant magnetization processes resulting from the non-ideal crystallographic structure of the material. Hence, while simulations on nanometer sized objects are performed to get an *exact* knowledge of the space and time behavior of the magnetization (mostly reversal) processes, the intended simulations on bulk like samples in the framework of electrical steels aim at distinguishing the different influences of the material parameters on the magnetic (hysteresis) processes. In this framework, it was already shown that the magnetization processes can be described on a somewhat larger space scale [1]. Now we also investigate how the accuracy of the computations influences the predicted macroscopic magnetic behavior.

In the micromagnetic theory the magnetic moments of the distinct atoms are homogenized to a continuum vector field which varies on a nanometer space scale [2]. This continuum field $\mathbf{M}(\mathbf{r},t)$ has a fixed, material dependent amplitude M_s, and a time and space varying orientation: $\mathbf{M}=M_s\mathbf{m}(\mathbf{r},t)$. The dynamics of the magnetic vector field are described by the Landau–Lifshitz equation. Different time stepping schemes, implicit [3,4] and explicit [5], are developed to integrate the Landau–Lifshitz equation. In these time stepping schemes, the interaction fields are evaluated several thousand times during one simulation. In practice, most of the CPU time goes to the evaluation of the magnetostatic field $\mathbf{H}_{ms}$ which describes the long range interactions in the ferromagnetic material. When the spatial discretization is performed using finite difference (FD) cells, fast Fourier transforms (FFTs) are widely used for the evaluation of $\mathbf{H}_{ms}$ (e.g. [6–8]).

In [9], two FFT based methods to compute the magnetostatic field in 2D structures are compared. The *constant magnetization*

* Corresponding author.
E-mail address: ben.vandewiele@ugent.be (B. Van de Wiele).

0304-8853/$ - see front matter © 2009 Elsevier B.V. All rights reserved.
doi:10.1016/j.jmmm.2009.09.077

method starts from a discretization where a uniform magnetization is assumed in each discretization cell. The *constant charge method* [10,11] starts from a discretization where a uniform magnetic charge density is assumed in each cell. In [9], the constant magnetization method is concluded to have superior convergence properties when edge and surface effects are important. In this paper, the constant magnetization method is used. Within this method, two approaches are adopted to compute the magnetostatic field.

In a first approach, an FFT based scheme evaluates the magnetostatic fields using the direct relation between $\mathbf{H}_{ms}$ and the uniform magnetization in each discretization cell. This FFT scheme provides results with a high accuracy. A second alternative FFT scheme evaluates, the magnetostatic field by taking the gradient of the scalar magnetic potential ψ_{ms} which is in turn computed using the relation between ψ_{ms} and the uniform magnetization in each discretization cell. This FFT scheme has a lower accuracy, but is faster and requires less memory. In this paper, the two FFT schemes are compared and evaluated in the framework of the micromagnetic hysteresis scheme [12], designed to investigate the relations between microstructure and macroscopic magnetic behavior. In [13,14] the validity and accuracy of the hysteresis scheme [12] is demonstrated.

In what follows, both schemes are summarized and their performance is evaluated. The influence of the low accuracy magnetostatic field evaluation on the simulated hysteresis behavior is determined and is compared with the influence of thermal fluctuations.

2. Magnetostatic field evaluation schemes

In the considered micromagnetic hysteresis model [12], the ferromagnetic sample is discretized using identical cubic FD cells as shown in Fig. 1. The magnetization is considered to be uniform in every FD cell. According to the micromagnetic theory, the amplitude of the magnetization is fixed $|\mathbf{M}| = M_s$ but the orientation can differ from cell to cell.

The magnetic moments of the FD cells interact with each other and with the local material properties. Classically, five different interaction terms are considered in the micromagnetic hysteresis scheme: the Zeeman interaction, the exchange interaction, the magnetostatic interaction, the anisotropy interaction and the magnetoelastic interaction. By time stepping the Landau–Lifshitz equation, the dynamic behavior in all N magnetization cells is simulated. Here, the corresponding interaction fields have to be evaluated several times. The evaluation of the magnetostatic field

$$\mathbf{H}_{ms}(\mathbf{r}) = -\frac{M_s}{4\pi}\int_{\Omega}\nabla\nabla\frac{\mathbf{m}(\mathbf{r}')}{|\mathbf{r}-\mathbf{r}'|}\,\mathrm{d}\mathbf{r}' \tag{1}$$

is the most time and memory intensive. In (1) Ω is the sample volume. Classically, the computations scale $\mathcal{O}(N^2)$. Numerical schemes based on FFTs accelerate these computations to $\mathcal{O}(N\log(N))$. Now two FFT based schemes to evaluate (1) are briefly outlined.

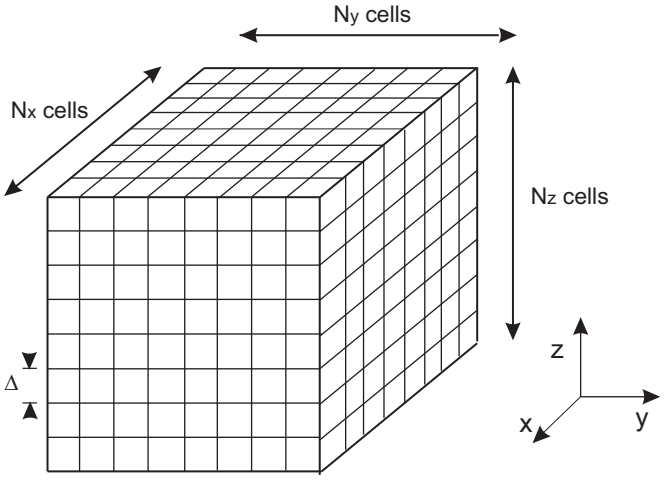

Fig. 1. Geometry discretization of a ferromagnetic sample.

2.1. Direct magnetostatic field evaluation (scheme 1)

In this approach, further referred to as *scheme* 1, expression (1) is evaluated directly. The magnetostatic field values have to be obtained in the center $\mathbf{r}_i$ of each FD cell $i = 1,\ldots,N$. The volume integral in (1) is split into N integrals over the volumes of the FD cells (with center $\mathbf{r}_j$, $j = 1,\ldots,N$). Since the magnetization is constant in each FD cell and all FD cells have the same volume V, $\mathbf{H}_{ms}$ can be rewritten as

$$\mathbf{H}_{ms}(\mathbf{r}_i) = -\frac{M_s}{4\pi}\sum_{\substack{j=1\\ j\neq i}}^{N}\int_V \nabla_{\boldsymbol{\rho}}\frac{\mathbf{r}_i-\mathbf{r}_j+\boldsymbol{\rho}}{|\mathbf{r}_i-\mathbf{r}_j+\boldsymbol{\rho}|^3}\,\mathrm{d}\boldsymbol{\rho}\cdot\mathbf{m}(\mathbf{r}_j). \tag{2}$$

The self-contribution to the magnetostatic field ($j = i$) is left out, according to [15]. Rewriting (2) explicitly as a convolution product yields

$$\mathbf{H}_{ms}(\mathbf{r}_i) = \sum_{\substack{j=1\\ j\neq i}}^{N}\mathbf{g}(\mathbf{r}_i-\mathbf{r}_j)\cdot\mathbf{m}(\mathbf{r}_j), \tag{3}$$

with $\mathbf{g}(\mathbf{r})$ the symmetrical Green's function tensor

$$\mathbf{g}(\mathbf{r}) = \begin{bmatrix} g_{xx}(\mathbf{r}) & g_{xy}(\mathbf{r}) & g_{xz}(\mathbf{r}) \\ g_{xy}(\mathbf{r}) & g_{yy}(\mathbf{r}) & g_{yz}(\mathbf{r}) \\ g_{xz}(\mathbf{r}) & g_{yz}(\mathbf{r}) & g_{zz}(\mathbf{r}) \end{bmatrix}. \tag{4}$$

Now, the discrete convolution theorem [16] is applied to the product (3):

$$\begin{aligned} \tilde{H}^{i,j,k}_{ms,x} &= \tilde{g}^{i,j,k}_{xx}\tilde{m}^{i,j,k}_{x} + \tilde{g}^{i,j,k}_{xy}\tilde{m}^{i,j,k}_{y} + \tilde{g}^{i,j,k}_{xz}\tilde{m}^{i,j,k}_{z}, \\ \tilde{H}^{i,j,k}_{ms,y} &= \tilde{g}^{i,j,k}_{xy}\tilde{m}^{i,j,k}_{x} + \tilde{g}^{i,j,k}_{yy}\tilde{m}^{i,j,k}_{y} + \tilde{g}^{i,j,k}_{yz}\tilde{m}^{i,j,k}_{z}, \\ \tilde{H}^{i,j,k}_{ms,z} &= \tilde{g}^{i,j,k}_{xz}\tilde{m}^{i,j,k}_{x} + \tilde{g}^{i,j,k}_{yz}\tilde{m}^{i,j,k}_{y} + \tilde{g}^{i,j,k}_{zz}\tilde{m}^{i,j,k}_{z}. \end{aligned} \tag{5}$$

Here, and in what follows, Fourier transformed quantities are denoted with a tilde. Following the convolution theorem, one computes the magnetostatic field by (i) Fourier transforming the magnetization data m_x, m_y and m_z after zero padding, (ii) performing the pointwise products (5) of the Fourier transformed magnetization data with the Fourier transformed Green's tensor elements (4) and (iii) inverse Fourier transforming the result of the previous step. Note that the zero padding is needed to exclude unwanted side effects originating from the cyclic nature of the FFTs. The elements in the Green's function matrices can be determined by evaluating the integrals in (2) using a Gaussian quadrature formula. When an adequate high order Gaussian quadrature formula is used to compute the elements of (4), the magnetostatic fields generated by the uniformly magnetized FD cells can be computed up to any wanted accuracy. In this work, a six digit accuracy is used since all other computations are single precision. The accuracy of the scheme is checked by comparison with analytical expressions provided in [17].

2.2. Magnetostatic field evaluation using the magnetic potential (scheme 2)

In this approach, further referred to as *scheme* 2, first the scalar magnetic potential $\psi_{ms}(\mathbf{r})$ is computed in each FD cell. Afterwards, the magnetostatic field is evaluated by taking the negative gradient of the magnetic potential

$$\mathbf{H}_{ms}(\mathbf{r}) = -\nabla\psi_{ms}(\mathbf{r}), \tag{6}$$

with

$$\psi_{ms}(\mathbf{r}) = \frac{M_s}{4\pi}\int_{\Omega'} \nabla\frac{\mathbf{m}(\mathbf{r}')}{|\mathbf{r}-\mathbf{r}'|}\,\mathrm{d}\mathbf{r}'. \tag{7}$$

The magnetic potential has to be obtained in the center $\mathbf{r}_i$ of each FD cell $i=1,\ldots,N$. As in Section 2.1 the volume integral is split into N integrals over the volumes of the FD cells (with center $\mathbf{r}_j$, $j=1,\ldots,N$). Since the magnetization is constant in each FD cell and all FD cells have the same volume V, the magnetic potential can be rewritten as

$$\psi_{ms}(\mathbf{r}_i) = \frac{M_s}{4\pi}\sum_{j=1}^{N}\int_V \nabla_{\boldsymbol{\rho}}\frac{1}{|\mathbf{r}_i-\mathbf{r}_j+\boldsymbol{\rho}|}\,\mathrm{d}\boldsymbol{\rho}\cdot\mathbf{m}(\mathbf{r}_j). \tag{8}$$

Rewriting (8) explicitly as a convolution product yields

$$\psi_{ms}(\mathbf{r}_i) = \sum_{j=1}^{N}\mathbf{f}(\mathbf{r}_i-\mathbf{r}_j)\cdot\mathbf{m}(\mathbf{r}_j), \tag{9}$$

with $\mathbf{f}(\mathbf{r})$ the Green's function vector

$$\mathbf{f}(\mathbf{r}) = [f_x(\mathbf{r})\ f_y(\mathbf{r})\ f_z(\mathbf{r})]. \tag{10}$$

Adopting the convolution theorem gives

$$\tilde{\psi}_{ms}^{i,j,k} = \tilde{f}_x^{i,j,k}\tilde{m}_x^{i,j,k} + \tilde{f}_y^{i,j,k}\tilde{m}_y^{i,j,k} + \tilde{f}_z^{i,j,k}\tilde{m}_z^{i,j,k}. \tag{11}$$

Hence, one computes the magnetic potential by (i) Fourier transforming the magnetization data m_x, m_y and m_z after zero padding in non-periodic directions, (ii) performing the pointwise products (11) of the Fourier transformed magnetization data with the Fourier transformed Green's vector elements (10) and (iii) inverse Fourier transforming the result of the previous step. Again, the elements in the Green's function vector can be determined by evaluating the integrals in (8) using a Gaussian quadrature formula or can be evaluated analytically in closed form [15].

To derive the magnetostatic field $\mathbf{H}_{ms}(\mathbf{r})$ in each FD cell (i,j,k) one has to take minus the gradient of the local magnetic potential $\psi_{ms}(\mathbf{r})$. This is approximated numerically using the following formula

$$\begin{bmatrix} H_{ms,x}^{i,j,k} \\ H_{ms,y}^{i,j,k} \\ H_{ms,z}^{i,j,k} \end{bmatrix} = \frac{1}{2\Delta}\begin{bmatrix} \psi_{ms}^{i-1,j,k} - \psi_{ms}^{i+1,j,k} \\ \psi_{ms}^{i,j-1,k} - \psi_{ms}^{i,j+1,k} \\ \psi_{ms}^{i,j,k-1} - \psi_{ms}^{i,j,k+1} \end{bmatrix}. \tag{12}$$

The self-contribution of each FD cell to the magnetic field in its center has to be subtracted in the last step of these computations. The numerical evaluation of the gradient (12) introduces discretization errors in the computed values of the magnetostatic fields.

3. Performance study

The memory requirements for both FFT based evaluation schemes are shown in Table 1. The different contributions are expressed in terms of *real* numbers. In both schemes $3N$ real numbers need to be saved for the magnetization data and the resulting magnetostatic field data. In schemes 1 and 2, the Fourier transformed Green's function elements are stored in, respectively, 6 and 3 matrices containing $4N$ *real* numbers. In scheme 1, $3\times 8N$ *real* numbers are required to store the $3\times 4N$ *complex* values of the Fourier transformed magnetization components while $8N$ real numbers suffice to store the pointwise products and inverse Fourier transforms in (5) successively for each magnetostatic field component. In scheme 2, the magnetization components M_q $(q=x,y,z)$ are Fourier transformed, multiplied pointwise with the corresponding Green's function matrix f_q and added to the Fourier transformed magnetic potential $\tilde{\psi}_{ms}$, one after the other, limiting the required memory for the Fourier transformed magnetization components to $4N$ *complex* values. In total the magnetostatic field evaluation scheme based on the magnetic potential requires about half of the memory compared to the direct evaluation scheme 1.

Table 1
Memory requirements expressed in real numbers for N FD cells.

	Scheme 1	Scheme 2
$\mathbf{m}$	$3\times N$	$3\times N$
$\mathbf{H}_{ms}$	$3\times N$	$3\times N$
$\tilde{\mathbf{g}}$ or $\tilde{\mathbf{f}}$	$6\times 4N$	$3\times 4N$
$\tilde{\mathbf{m}}$	$3\times 8N$	$1\times 8N$
$\tilde{\mathbf{H}}_{ms}$ or $\tilde{\psi}_{ms}$	$1\times 8N$	$1\times 8N$
Total	$62N$	$34N$

Table 2
Computations for the evaluation of $\mathbf{H}_{ms}$ for N FD cells.

	Scheme 1	Scheme 2
Forward FFTs	3	3
Pointwise products	$9\times 4N$	$3\times 4N$
Inverse FFTs	3	1
Gradients	0	N

The computations needed for the evaluation of $\mathbf{H}_{ms}$ per time step are shown in Table 2 for both schemes. In both schemes all three zero padded magnetization matrices are Fourier transformed. In scheme 1, $9\times 4N$ *real* $\times$ *complex* multiplications are performed to evaluate the pointwise products (5), while scheme 2 only needs $3\times 4N$ *real* $\times$ *complex* multiplications to evaluate (11). The first scheme needs three inverse Fourier transforms while the second scheme only needs one. Additionally, in the FFT scheme based on the magnetic potential, the gradient of the magnetic potential ψ_{ms} has to be evaluated in every FD cell. This leads to a CPU time reduction for the magnetostatic field evaluation scheme 2 based on the magnetic potential of 65% compared with the direct evaluation scheme 1.

Due to the numerical gradient evaluation of the gradient (12), scheme 2 is expected to have a lower accuracy compared to scheme 1. The accuracy of the magnetic potential based FFT scheme is determined by comparing the magnetostatic field values obtained by both schemes for iron monocrystals of different dimensions in a micromagnetic equilibrium state encountered in the simulation of their hysteresis loop. The normalized error, defined as

$$\text{error} = \sqrt{\frac{\sum_{i=1}^{N}|\mathbf{H}_{ms,i}^{FFT2}-\mathbf{H}_{ms,i}^{FFT1}|^2}{\sum_{i=1}^{N}|\mathbf{H}_{ms,i}^{FFT1}|^2}} \tag{13}$$

is shown in Table 3 for different sample dimensions. The fields $\mathbf{H}_{ms}^{FFT1}$, computed in scheme 1 are considered as a reference. Table 3 shows that the error decreases for larger sample dimensions to less than one percent. This is because in larger monocrystals the magnetostatic potential is smoother than in the small

monocrystals. This results in a more accurate numerical approximation of the gradient (12). To demonstrate this Fig. 2 shows magnetic configurations in different planes of the sample with edges of 1.28 μm together with the magnetostatic field values and the local normalized error in the same planes. As expected, the largest errors occur near the domain walls where the variations of the magnetic potential are larger leading to larger errors on the magnetostatic field values. Furthermore, it should be noted that higher order approximations for the gradient operator only lead to small improvements in accuracy.

4. Hysteresis simulation

When considering hysteresis properties, one is predominantly interested in magnetization process in micromagnetically large objects with dimensions in the order of micrometers and larger. On this space scale the study of magnetization processes is typically based on the domain theory [18]. Here, uniform magnetization regions are assumed through the complete sample. Since this assumption is not always valid, micromagnetic simulations should be able to validate and probably improve the results obtained by the domain theory. Ideally, the micromagnetic computations should be worked out with the same spatial and numerical accuracy as used in the 'classical' micromagnetic research domains.

Table 3
Accuracy of scheme 2 for different dimensions.

Edge size (μm)	Normalized error
0.32	0.0250
0.64	0.0124
1.28	0.0056
2.56	0.0031

Classically, the discretization size is imposed by the exchange length. Together with a careful description of the exchange interaction this guarantees the *most accurate* simulation of the magnetization processes in the small magnetic samples under study [19,20]. In micromagnetic (hysteresis) simulations that describe magnetization processes in much larger non-ideal ferromagnetic samples, the accuracy which is aimed at is much lower, particulary because the materials' microstructure itself is only known to a certain extend. In this case, the use of a discretization size larger than the exchange length corresponds to a low level homogenization. The resulting low accuracy evaluation of the exchange interaction has only a limited influence on the macroscopic magnetic (hysteresis) properties under study, but vastly accelerates the computations [1]. The limited impact on the magnetization curves can be understood by the fact that in large ferromagnetic samples where domains determine the magnetization processes, the exchange interactions are much less dominant, compared to the magnetization processes in classical small magnetic samples where vortex magnetization states are more present.

In this context, the question arises to what extend the use of the lower accuracy $\mathbf{H}_{ms}$ evaluation scheme influences the simulated macroscopic hysteresis behavior of micrometer sized samples. To investigate the impact of the lower accuracy evaluation of $\mathbf{H}_{ms}$, the micromagnetic hysteresis scheme [12] is used. We recall that the hysteresis loop is obtained as an assembly of successive equilibrium states and that the Landau–Lifshitz equation is time stepped to go from one equilibrium state to the next one. As an example, elongated iron samples ($\mu_0 M_s = 2.1\,\mathrm{T}$)

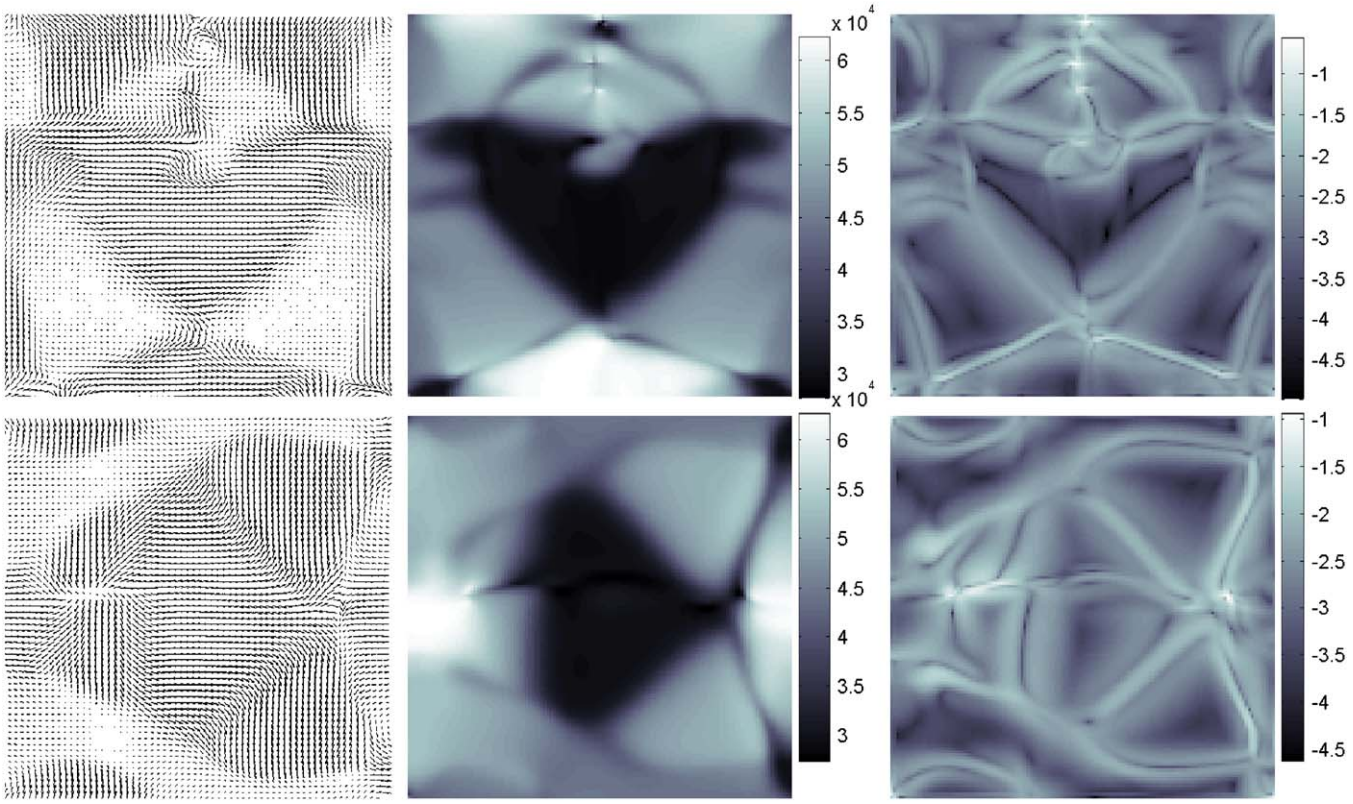

Fig. 2. Locally averaged magnetization (left), amplitude of the magnetostatic field [$\mathrm{A\,m^{-1}}$] (middle) and local normalized error on a logarithmic scale (right) in planes $x = 0.16\,\mu\mathrm{m}$ (up) and $z = 0.16\,\mu\mathrm{m}$ (down) of an iron cubic sample with edges of 1.28 μm.

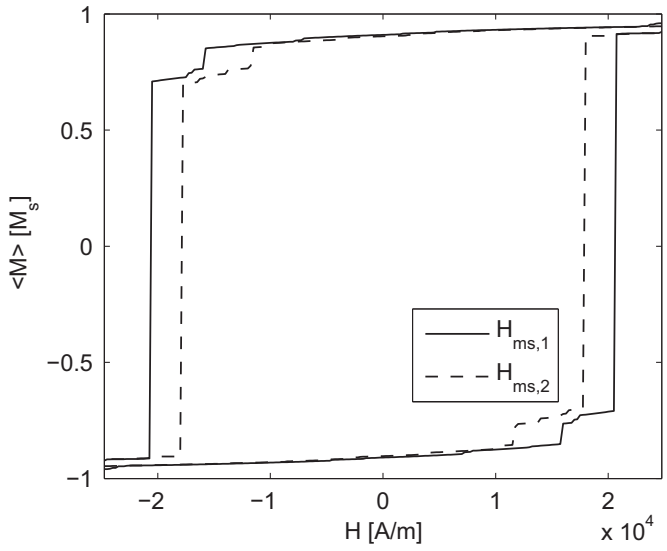

Fig. 3. Hysteresis loops for a ferromagnetic sample A with dimensions $0.5\,\mu m \times 0.5\,\mu m \times 16.0\,\mu m$, computed using the high accuracy $\mathbf{H}_{ms}$ evaluation scheme 1 (full line) and the magnetic potential based $\mathbf{H}_{ms}$ evaluation scheme 2 (dashed line).

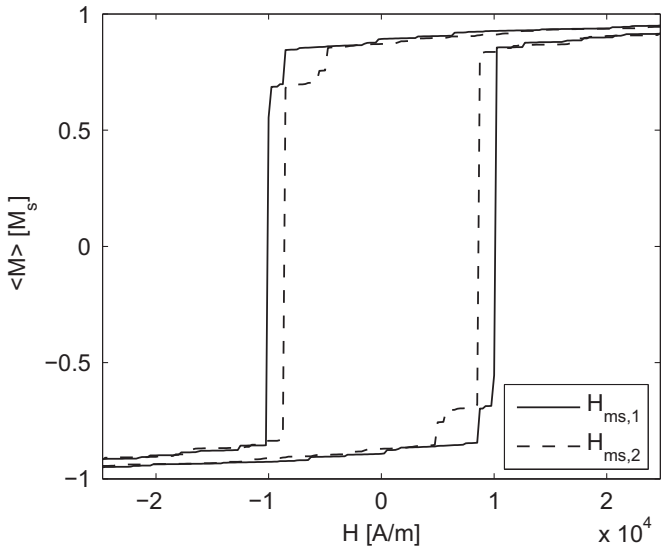

Fig. 4. Hysteresis loops for a ferromagnetic sample B with dimensions $1.0\,\mu m \times 1.0\,\mu m \times 32.0\,\mu m$, computed using the high accuracy $\mathbf{H}_{ms}$ evaluation scheme 1 (full line) and the magnetic potential based $\mathbf{H}_{ms}$ evaluation scheme 2 (dashed line).

with dimensions $0.5\,\mu m \times 0.5\,\mu m \times 16.0\,\mu m$, $1.0\,\mu m \times 1.0\,\mu m \times 32.0\,\mu m$ and $1.5\,\mu m \times 1.5\,\mu m \times 48.0\,\mu m$ are considered, discretized using 10 nm sized FD cells leading to 4 000 000, 32 000 000 and 108 000 000 FD cells, respectively. All samples contain 32 grains with cubic anisotropy axes. Here, random stresses are added to simulate the grain boundaries. In what follows, the samples will be referred to as *samples A, B* and *C*, respectively. The semi-analytical predictor-corrector scheme [5] is used to time step the Landau–Lifshitz equation that describes the evolution towards equilibrium states at successive constant values of the external field, applied along the longest direction of the sample. All simulations are performed using a multithreaded implementation on an AMD Opteron 2350 machine (4×2 cores) with 32 GB of shared memory.

4.1. *Influence of low accuracy* $\mathbf{H}_{ms}$ *evaluation*

The resulting hysteresis loops with the magnetostatic field computed using schemes 1 and 2 are shown in Fig. 3–5. Due to the elongated shape of the sample, the hysteresis loops take a large jump at the coercive field. In both Figs. 3 and 4 the coercive field values for the loops simulated with the high accuracy $\mathbf{H}_{ms}$ evaluation scheme 1 are larger than the corresponding loop simulated with the lower accuracy $\mathbf{H}_{ms}$ evaluation scheme 2. This is understood as follows. When saturated at high (positive) external fields, the samples are in a stable micromagnetic equilibrium state. Diminishing the applied field makes the systems evolve from these stable states to metastable equilibrium states. When the applied field corresponds with the coercive field, domain structures are initiated which enable the magnetic system to reverse to the opposite magnetization state. The domain nucleation, needed to initiate such a domain structures, typically originates at points where small variations occur in the quantities describing the magnetic sample. If these variations are absent, large opposite external fields are required to initiate the reversal process. In the hysteresis loops based on the lower accuracy $\mathbf{H}_{ms}$ evaluation scheme 2, the numerical noise on the magnetostatic fields account for the small variations that nucleate the domain structure. In the loops simulated with the high accuracy $\mathbf{H}_{ms}$ evaluation scheme 1, such variations are absent

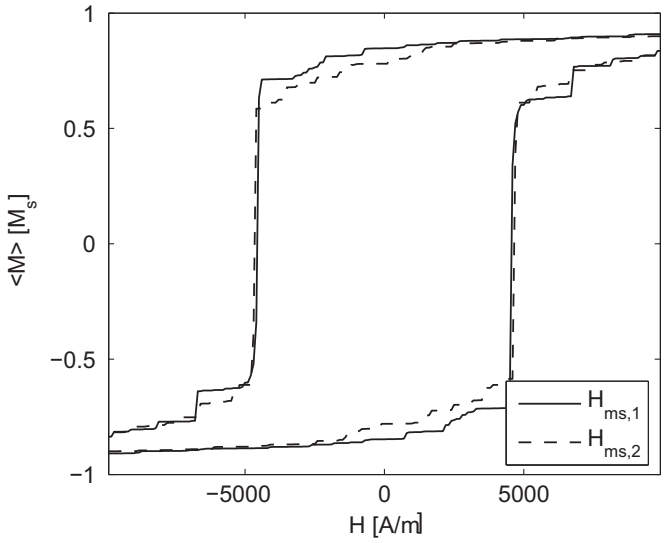

Fig. 5. Hysteresis loops for a ferromagnetic sample C with dimensions $1.5\,\mu m \times 1.5\,\mu m \times 48.0\,\mu m$, computed using the high accuracy $\mathbf{H}_{ms}$ evaluation scheme 1 (full line) and the magnetic potential based $\mathbf{H}_{ms}$ evaluation scheme 2 (dashed line).

and a higher opposite applied field is needed to initiate the magnetization reversal.

The coercive fields for the simulated hysteresis loops of the largest sample C have identical values and the resulting loops are very similar (see Fig. 5). However, the above reasoning still holds. Here, the micromagnetic equilibrium states before the reversal point are more stable and the numerical noise has only little influence. It is only at the coercive field that in both simulations domains are initiated leading to the magnetization reversal.

The stability of the successive micromagnetic equilibrium states is also expressed by the number of time steps needed to time step the Landau–Lifshitz equation (and consequently the CPU time) between successive equilibrium states during the simulation of the hysteresis loops. The number of times steps δt are given in Table 4, together with the CPU time and the memory requirements for the discussed simulations. For the loops of

Table 4
Simulation data: hysteresis loops with different $\mathbf{H}_{ms}$ evaluation schemes.

Simulation	δt	CPU time	Mem. (GB)
Sample A, scheme 1	1461	1 h 5 min	1.1
Sample A, scheme 2	1796	1 h 5 min	0.65
Sample B, scheme 1	4447	24 h 22 min	8.9
Sample B, scheme 2	6378	29 h 18 min	5.5
Sample C, scheme 1	11219	236 h 20 min	30.0
Sample C, scheme 2	11388	212 h 31 min	18.7

samples A and B, more time steps are needed when the low accuracy $\mathbf{H}_{ms}$ evaluation scheme 2 is used. Indeed, due to the introduced numerical noise, the micromagnetic systems converge slower to the successive metastable equilibrium states when the lower accuracy $\mathbf{H}_{ms}$ evaluation scheme 2 is used. This is not the case for the hysteresis simulation of sample C. As outlined above, the successive equilibrium states are more stable, enabling the system to converge fast to the next equilibrium state despite the numerical noise.

From Table 4 it is also clear that when the $\mathbf{H}_{ms}$ evaluation scheme 2 is introduced in the micromagnetic hysteresis model [12] instead of scheme 1 (i) the CPU time to compute a time step is reduced with about 15% and (ii) the memory requirements are reduced with 37%. A possible gain in the total CPU time depends on the stability of the system in every point of the hysteresis loop. Furthermore, one can conclude that for growing sample sizes (i) the number of time steps in the hysteresis simulation grows and (ii) the coercive fields diminish (see Figs. 3–5).

4.2. Influence of thermal fluctuations

Now, comparison is made with the influence of thermal fluctuations on the hysteresis behavior of the ferromagnetic samples. Therefore a random thermal fluctuation field [21] is added in the micromagnetic description. The thermal field $\mathbf{H}_{th}$ is assumed to be a Gaussian random process with zero mean value in each direction $q = x, y, z$ and to be uncorrelated in both space and time

$$\langle H_{th,q}(\mathbf{r}, t)\rangle = 0, \tag{14}$$

$$\langle H_{th,p}(\mathbf{r}, t) H_{th,q}(\mathbf{r}', t')\rangle = 2D\delta_{pq}\delta(\mathbf{r} - \mathbf{r}')\delta(t - t'). \tag{15}$$

The amplitude of the thermal fluctuations is derived from the fluctuation-dissipation theorem

$$D = \frac{\alpha k_B T}{|\gamma_G|\mu_0 M_s \Delta^3}, \tag{16}$$

with α the damping constant, k_B the Boltzmann constant, T the temperature, γ_G the gyromagnetic ratio and μ_0 the vacuum permeability. Hence, the thermal field can be expressed as

$$\mathbf{H}_{th} = \boldsymbol{\eta}(\mathbf{r}, t)\sqrt{\frac{2\alpha k_B T}{|\gamma_G|\mu_0 M_s \Delta^3 \delta t}}, \tag{17}$$

with δt the used time step and $\boldsymbol{\eta}(\mathbf{r}, t)$ a stochastic vector whose components are Gaussian random numbers, uncorrelated in space and time, with zero mean value and dispersion 1. In the semi-analytical predictor-corrector time stepping scheme, $\mathbf{H}_{th}$ is added to the other effective field terms, so no changes in the time stepping algorithm are required.

In the considered simulations, the damping constant α is 0.02, the FD cell size $\Delta = 10$ nm and the used time step δt is 2.5 ps. It is known that the above introduced thermal fluctuations make it possible to overcome energy barriers in the micromagnetic energy landscape of the considered ferromagnetic system. The larger the amplitude of the thermal fluctuations, the larger the energy barriers that can be overcome. Figs. 6–8 show the simulated hysteresis loops for the ferromagnetic samples considered above. Here, the high accuracy magnetostatic field evaluation scheme 1 is used. The fluctuating thermal fields correspond with different temperatures (0, 210, 260, 310 and 360 K). It is clear that for $T = 0$ K the thermal fields are zero and the resulting hysteresis loops correspond to the ones simulated in Section 4.1.

Figs. 6 and 7 show the hysteresis loops corresponding with samples A and B. As expected, higher temperatures result in lower coercive field values. Indeed, at higher temperatures, the amplitude of the fluctuations rises, enabling the system to overcome larger energy barriers, resulting in a possible domain nucleation in more stable energy states. Hence, the magnetization reversal can take place at smaller applied fields. The hysteresis loops at different temperatures for sample C with

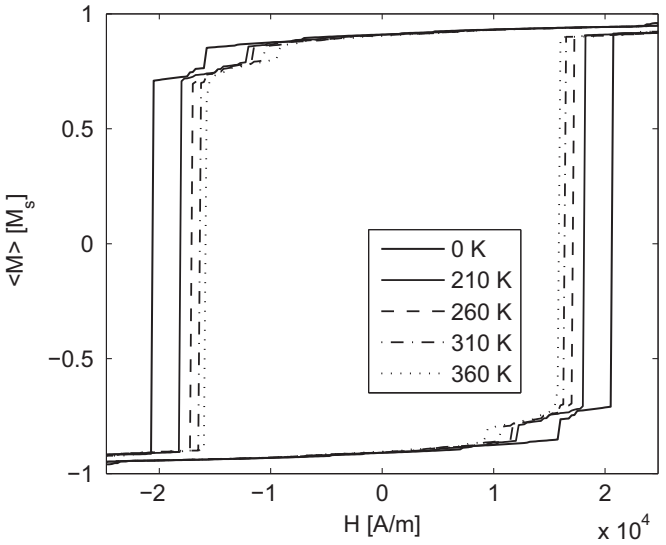

Fig. 6. Hysteresis loops for the same ferromagnetic sample as in Fig. 3 (sample A), computed using $\mathbf{H}_{ms}$ scheme 1. Thermal effects are taken into account for different temperatures.

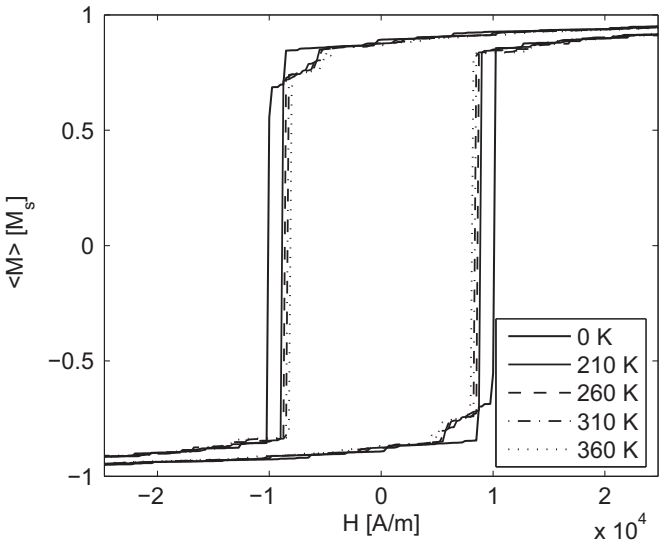

Fig. 7. Hysteresis loops for the same ferromagnetic sample as in Fig. 4 (sample B), computed using $\mathbf{H}_{ms}$ scheme 1. Thermal effects are taken into account for different temperatures.

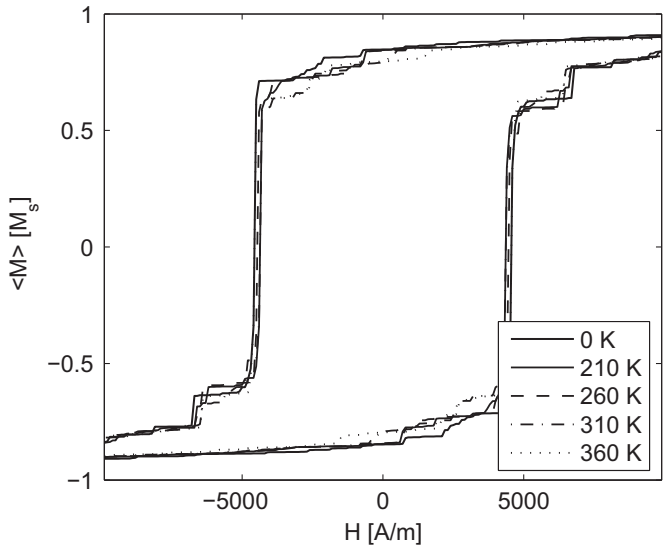

Fig. 8. Hysteresis loops for the same ferromagnetic sample as in Fig. 5 (sample C), computed using $\mathbf{H}_{ms}$ scheme 1. Thermal effects are taken into account for different temperatures.

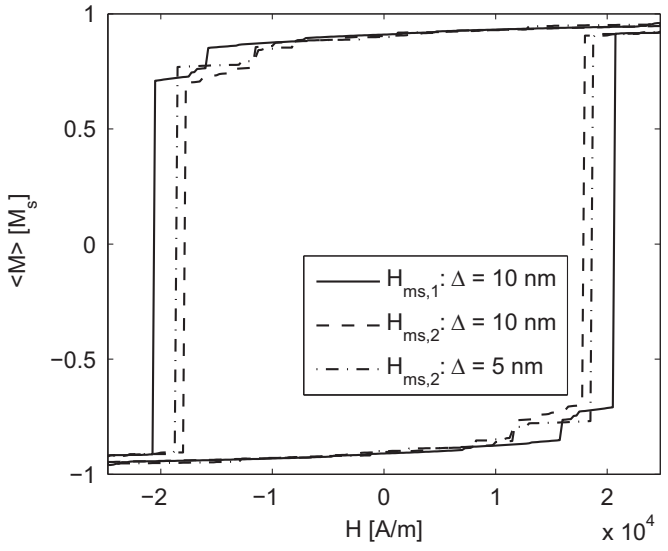

Fig. 9. Hysteresis loops for sample A, computed using $\mathbf{H}_{ms}$ scheme 1, $\mathbf{H}_{ms}$ scheme 2 with discretization size $\Delta = 10$ nm and $\mathbf{H}_{ms}$ scheme 2 discretization size $\Delta = 5$ nm.

Table 5
Simulation data: hysteresis loops for different temperatures.

Simulation	δt	CPU time
Sample A, 0 K	1461	1 h 5 min
Sample A, 210 K	1639	1 h 12 min
Sample A, 260 K	1825	1 h 19 min
Sample A, 310 K	1827	1 h 20 min
Sample A, 360 K	2159	1 h 34 min
Sample B, 0 K	4447	24 h 22 min
Sample B, 210 K	5790	37 h 49 min
Sample B, 260 K	5643	36 h 52 min
Sample B, 310 K	5753	37 h 35 min
Sample B, 360 K	6328	42 h 11 min
Sample C, 0 K	11219	236 h 20 min
Sample C, 210 K	13220	262 h 11 min
Sample C, 260 K	11479	228 h 8 min
Sample C, 310 K	12466	246 h 44 min
Sample C, 360 K	12487	247 h 35 min

dimensions $1.5\,\mu\text{m} \times 1.5\,\mu\text{m} \times 48.0\,\mu\text{m}$ shown in Fig. 8 are almost identical. Since the successive equilibrium states are more stable compared with the ones in samples A and B, the thermal fluctuations only have a negligible influence on the hysteresis loop. For applied fields somewhat smaller than the coercive field, the energy barriers are still too large to be overcome by the thermal fluctuations and to initiate the magnetization reversal.

In these simulations, the temperature can also have a large impact on the number of time steps and thus on the CPU time. This is shown in Table 5. For samples A and B, the number of time steps δt increases for higher temperatures, while this is much less pronounced for sample C. In samples A and B, higher temperatures (i.e. rising amplitudes of the fluctuating thermal field) make the micromagnetic systems converge slower to successive equilibrium points. The larger fluctuations open up a higher number of possible energy paths between successive (metastable) equilibrium points, resulting in more time steps and larger CPU times. For the hysteresis simulation of sample C, the successive equilibrium states are more stable and the energy paths between the equilibrium states are more confined. Hence the thermal fluctuations do not have a large impact on the total number of time steps.

4.3. Comparison

Now we can compare the results described in Sections 4.1 and 4.2. In both simulation series, noise terms of very different origin influence the hysteresis behavior. For a given magnetic configuration, the numerical noise in Section 4.1 is constant, while the thermal noise still depends on the used time step δt and discretization size Δ, see expression (17). However, similar conclusions can be drawn concerning their influence. Indeed, the same mechanisms are at the origin of the possible variations of the coercive fields. The numerical noise on the $\mathbf{H}_{ms}$ evaluation on the one hand and the thermal fluctuations on the other hand, can initiate domain nucleation at smaller applied fields compared with the loops computed with the high accuracy $\mathbf{H}_{ms}$ evaluation scheme at $T = 0$ K. The possible reduction of the coercive field depends in both cases on the stability of the equilibrium states in every point of the hysteresis loop. From Tables 4 and 5 it is also clear that given a micromagnetic system, the low accuracy evaluation of $\mathbf{H}_{ms}$ or the addition of thermal fluctuations has the same impact on the number of time steps required for the simulation of the hysteresis loop. When the systems runs through metastable equilibrium states, more time steps are required in both cases.

When thermal fluctuations are considered in a certain sample, the coercive field $H_c(T)$ increases monotonically to $H_c(T = 0)$ for decreasing temperatures and thus decreasing amplitudes of the thermal field $\mathbf{H}_{th}$. In the same way, smaller numerical noise levels should lead to increasing coercive fields, converging to $H_c(T = 0)$ when numerical noise is zero. To examine this, the simulations of Fig. 3 on sample A are rerun with the $\mathbf{H}_{ms}$ evaluation scheme 2. The discretization, however, is refined to FD cells with halved dimensions ($\Delta = 5$ nm) leading to a higher precision. The hysteresis loop is shown in Fig. 9 together with the loops of Fig. 3 ($\Delta = 10$ nm, $\mathbf{H}_{ms}$ evaluated with schemes 1 and 2). From Fig. 9 it is clear that, as expected, the hysteresis loop simulated with $\mathbf{H}_{ms}$ scheme 2 and $\Delta = 5$ nm has an intermediate coercive field, since the magnetostatic field evaluations in the considered simulation have also an intermediate precision.

When we interpret these results in the framework of the micromagnetic hysteresis modeling we can see that the hysteresis loops in Fig. 9 are very similar, but not identical. Indeed, on the microscopic level, the space and time behavior of the magnetiza-

tion is slightly different. However, it is clear that the same magnetic processes dominate the hysteresis behavior of the ferromagnetic sample and identical conclusions concerning the macroscopic magnetic behavior can be drawn independent of the used $\mathbf{H}_{ms}$ evaluation scheme. This shows that the low accuracy $\mathbf{H}_{ms}$ evaluation scheme can be used in micromagnetic hysteresis simulations. Furthermore, the origin of the small variations in the hysteresis loops is now clarified: the introduced numerical noise initiates the domain reversal at smaller coercive fields and larger numerical noise levels give rise to smaller coercive fields. Although the numerical noise is not Gaussian distributed and is not uncorrelated in space and time, these conclusions are identical to the conclusions drawn from simulations with additional thermal noise. Indeed, the influence of the thermal fluctuations depends in the same way on the stability of the successive micromagnetic equilibrium points. Moreover, the differences in the hysteresis loops simulated with the low accuracy $\mathbf{H}_{ms}$ evaluation scheme are of the same magnitude as encountered when thermal fluctuations for moderate temperatures are taken into account.

5. Conclusions

In micromagnetic hysteresis modeling one aims to relate microstructural material features with macroscopic magnetic behavior. Here, the evaluation of the magnetostatic field determines the performance of the used numerical scheme. Two FFT based schemes for the evaluation of magnetostatic fields are presented. The first scheme has an accuracy corresponding with the machine precision, while the second scheme is less accurate, but significantly reduces the memory requirements and CPU time for one magnetostatic field evaluation. The influence on the simulated hysteresis loops is investigated. Applying the low accuracy $\mathbf{H}_{ms}$ evaluation scheme results in a total memory reduction to 63% of the high accuracy calculation, but can introduce some differences in the shape of the hysteresis loops. To interpret these differences comparison is made with the influence of thermal effects. It is found that the deviations introduced by the numerical noise on the $\mathbf{H}_{ms}$ evaluation on the one hand and by the thermal fluctuations on the other hand, both find their origin in the stability of the magnetization states between successive equilibrium points. The resulting differences in the macroscopic (hysteresis) behavior, introduced by the numerical noise, are of the same magnitude as those when taking thermal fluctuations into account with moderate temperatures.

Acknowledgments

This work was supported by the Institute for the Promotion of Innovation through Science and Technology in Flanders (IWT-Vlaanderen) SB/53032 and also by FWO project G.0142.08.

References

[1] B. Van de Wiele, L. Dupré, F. Olyslager, Physica B 403 (2008) 372–375.
[2] H. Kronmüller, M. Fähnle, Micromagnetism and the Microstructure of Ferromagnetic Solids, Cambridge University Press, Cambridge.
[3] M. d'Aquino, C. Serpico, G. Miano, J. Comput. Phys. 209 (2) (2005) 730–753.
[4] X.P. Wang, C.J. Garcia-Cervera, E. Weinan, J. Comput. Phys. 171 (2001) 357–372.
[5] B. Van de Wiele, F. Olyslager, L. Dupré, IEEE Trans. Magn. 43 (6) (2007) 2917–2919.
[6] W. Rave, K. Fabian, T. Leibl, A. Hubert, J. Magn. Magn. Mater. 190 (1998) 332–348.
[7] S.W. Yuan, H.N. Bertram, IEEE Trans. Magn. 28 (5) (1992) 2031–2036.
[8] D.V. Berkov, J. Magn. Magn. Mater. 161 (1996) 337–356.
[9] R.D. McMichael, M.J. Donahue, G. Porter, J. Appl. Phys. 85 (8) (1999) 5816–5818.
[10] K. Ramstöck, T. Leibl, A. Hubert, J. Magn. Magn. Mater. 135 (1) (1994) 97–110.
[11] D.V. Berkov, K. Ramstöck, A. Hubert, Phys. Status Solidi A 137 (1) (1993) 207–225.
[12] B. Van de Wiele, F. Olyslager, L. Dupré, J. Appl. Phys. 101 (2007) 07390.
[13] B. Van de Wiele, A. Manzin, O. Bottauscio, M. Chiampi, L. Dupré, F. Olyslager, IEEE Trans. Magn. 44 (11) (2008) 3137–3140.
[14] B. Van de Wiele, A. Manzin, L. Dupré, F. Olyslager, O. Bottauscio, M. Chiampi, IEEE Trans. Magn. 45 (3) (2009) 1614–1617.
[15] M.E. Schabes, A. Aharoni, IEEE Trans. Magn. 23 (6) (1987) 3882–3888.
[16] W.H. Press, S.A. Teukolsky, W.T. Vetterling, B.P. Flannerly, Numerical Recipes in C: The Art of Scientific Computing, Cambridge University Press, Cambridge, 1995.
[17] A. Aharoni, J. Appl. Phys. 83 (6) (1998) 3432–3434.
[18] A. Hubert, R. Schäfer, Magnetic Domains, Springer, Berlin, 1998.
[19] M.J. Donahue, J. Appl. Phys. 83 (11) (1998) 6491–6493.
[20] M.J. Donahue, D.G. Porter, Physica B 343 (2004) 177–183.
[21] W.F. Brown, Phys. Rev. 130 (5) (1963) 1677–1686.